

AUTOMATED YIELD MAP DELAY IDENTIFICATION USING PHASE CORRELATION METHODOLOGY

D. H. Lee, K. A. Sudduth, S. T. Drummond, S. O. Chung, D. B. Myers

ABSTRACT. *Crop yield data are a key component of precision agriculture and are critical for both development and evaluation of precision management strategies. Ideally, software that generates grain yield maps from raw yield monitor data should automatically correct errors associated with machine and operating characteristics. Perhaps the most basic correction required is to properly compensate for the time lag (or position lag) between the cutting of the crop from the field and the grain flow measurement by the flow sensor in the combine. Past research has suggested several approaches to automatically determine delay time, but for various reasons these have not been implemented in mapping software. In this article, we present a new, computationally efficient method that can accurately determine delay time for individual fields using the image processing method of phase correlation. The phase correlation delay identification (PCDI) method was evaluated using a number of yield maps with varying degrees of harvest complexity, and results were compared to a geostatistical method. The PCDI method produced accurate estimates of delay time in approximately 90% of test datasets and provided a way to evaluate the reliability of the estimate. Additionally, the PCDI method was more computationally efficient than previous methods. Results of this study will increase the feasibility of including automatic delay time compensation in yield mapping software.*

Keywords. *Delay time, Geostatistical analysis, Phase correlation, Precision agriculture, Spatial consistency, Yield map.*

Yield mapping based on data from yield monitoring systems has become a key tool of precision agriculture. Yield mapping is critical in helping the producer to identify the location of problem areas in spatially variable fields. It assists in defining the magnitude of these problems, which is important for both diagnosis and management decisions. Lastly, it is useful in the economic analysis of any management changes the producer might decide to implement (Massey et al., 2008).

The creation of high-accuracy yield maps from combine grain harvester yield monitor system data is complicated by a variety of factors. Foremost among these is the fact that the transport time of the grain through the header, the

threshing mechanism, and up the clean grain elevator to the grain flow sensor is significant. Furthermore, these transport delays vary between crops, between harvesters, and under different harvesting conditions. Several researchers (Blackmore and Marshall, 1996; Lamb et al., 1997; Chung et al., 2002) have mentioned the importance of accurately identifying and correcting for this grain flow delay time, and it has been noted that these errors can result in both inaccurate estimates of crop yield and positional offsets of those estimates (Moore, 1998).

Some researchers have suggested systems that could minimize the effect of the transport delay by changing the location of the grain flow measurement (e.g., Veal et al., 2010). Others have investigated deconvolution of the grain flow signal using a dynamic model (Whelan and McBratney, 2002; Arslan and Colvin, 2002), although Birrell et al. (1996) found no practical advantage in this approach. The more common approach in practice has been to estimate a simple, fixed delay time for a particular dataset, generally by visual inspection of yield maps (e.g., Stott et al., 1993; Robinson and Metternicht, 2005; Reyniers and De Baerdemaeker, 2005; Sudduth and Drummond, 2007). Chung et al. (2002) and Sudduth and Drummond (2007) present figures that allow visualization of yield maps with correct and incorrect delay time choices.

To reduce subjectivity compared to the visual inspection approach, several research groups introduced post-processing methods to estimate delay time. Yang et al. (2002) tried to maximize the correlation between in-season airborne multispectral imagery and yield maps with various delays to determine which time lag was appropriate. Beal and Tian (2001) looked at the surface area ratios of gridded

Submitted for review in October 2011 as manuscript number PM 9455 approved for publication by the Power & Machinery Division of ASABE in May 2012. Presented at the 2011 ASABE Annual Meeting as Paper No. 1111626.

Mention of trade names or commercial products is solely for the purpose of providing specific information and does not imply recommendation or endorsement by the USDA or its cooperators. The USDA is an equal opportunity provider and employer.

The authors are **Dong-Hoon Lee**, Visiting Scholar, Department of Biological Engineering, **Kenneth A. Sudduth**, ASABE Fellow, Research Agricultural Engineer, USDA-ARS Cropping Systems and Water Quality Research Unit (CSWQRU), and **Scott T. Drummond**, Information Technology Specialist, USDA-ARS CSWQRU, University of Missouri, Columbia, Missouri; **Sun-Ok Chung**, ASABE Member, Assistant Professor, Department of Biosystems Machinery Engineering, Chungnam National University, Daejeon, South Korea; and **D. Brenton Myers**, Research Soil Scientist, USDA-ARS CSWQRU, University of Missouri, Columbia, Missouri. **Corresponding author:** Kenneth A. Sudduth, USDA-ARS CSWQRU, 269 Agricultural Engineering Bldg., University of Missouri, Columbia, MO 65211; phone: 573-882-1114, ext. 303; e-mail: Ken.Sudduth@ars.usda.gov.

yield maps representing a set of potential delay times and found the best results, in comparison to visual inspection of yield maps, when this ratio was minimized. Our previous research (Chung et al., 2002) used both geostatistical (minimal nugget) and segmentation (minimal quad-tree decomposition) methods to compute delay times for both flow and moisture sensors and compared them to delay times estimated by visual methods. Both methods worked well, with results that generally agreed within 1 s to those obtained by visual inspection.

While various commercial and research software packages are available to help detect and/or remove many error types affecting yield map accuracy (e.g., Sudduth and Drummond, 2007), fully automated detection and correction of delay times has not been implemented. If an automated method is to prove useful, it will need to exhibit the following three traits: it must be reliably accurate, it must be computationally inexpensive, and it must require only minimal user input to complete.

Incorrect delay times cause periodic error patterns in yield maps due to the generally used back-and-forth harvesting pattern. This “sawtooth” pattern, previously described by many authors including Chung et al. (2002) and Sudduth and Drummond (2007), is the basic diagnostic feature used in the visual inspection method. Because of the periodicity imparted by the harvesting pattern, we hypothesized that certain frequency domain image processing techniques might be useful in identifying the appropriate delays. Frequency domain analysis has been commonly used to identify similarity or periodic patterns within digital images (Broughton and Bryan, 2008). One such technique, phase correlation, was found to be the most robust method to estimate the relative translational offset between two similar images (De Castro and Morandi, 1987).

In this article, we develop a method for detecting delay times based primarily on the use of phase correlation. The method was applied to a variety of spatial datasets to ensure that it was computationally efficient and robust. Our objectives were to evaluate whether the technique could accurately determine delay times, and to determine if it could be used to automate the process of determining delay time.

MATERIALS AND METHODS

DATASETS USED

Six sets of yield data used in our prior related research (Sudduth and Drummond, 2007; Chung et al., 2002) were chosen for initial development of our method for detecting delay time. The datasets were selected to include variations in field size, harvest complexity (a qualitative indication of how many different harvest directions and sections were present in the field), crop, and level of yield variability. Table 1 documents the information regarding the sites, as well as summary data related to each dataset.

Datasets 1, 4, and 6 represent relatively large fields, with very flat topography and simple harvest patterns. Datasets 3 and 5 represent the other extreme: relatively smaller fields having low yields (soybean) and relatively more complex harvest patterns. Dataset 2 includes extremely rolling to-

Table 1. Descriptive statistics for the six test fields.

Statistic	Dataset					
	1	2	3	4	5	6
Slope	0% to 2%	2% to 6%	0% to 1%	0% to 1%	1% to 2%	0% to -2%
Terraced	No	Yes	No	N	No	No
Size (ha)	21	18	15	48	11	36
Complexity	Low	High	Medium	Low	High	Low
Crop	Corn	Corn	Soybean	Corn	Soybean	Corn
Exported delay (s)	0	12	12	12	12	12
Raw mean (Mg ha ⁻¹)	4.74	8.06	2.56	11.07	2.42	4.62
Raw SD (Mg ha ⁻¹)	2.82	2.73	1.19	3.35	0.87	1.70
Number of data points	36,816	19,495	11,010	66,188	9,333	38,459

pography, along with relatively high yields (corn) and a very complex harvest pattern. Each site was harvested using a combine instrumented with a calibrated AgLeader yield monitoring system. Combine header widths ranged from 4.5 to 6 m on the corn sites and from 7 to 9 m on the soybean sites. Once the data were collected and archived using AgLeader SMS Basic software, an AgLeader advanced dataset was exported for each field. For datasets 2 through 6, the flow delay used for export was 12 s, and the start pass and end pass delays, which are used to delete inaccurately low yields obtained as the harvester threshing mechanism fills at the beginning and empties at the end of each pass, were set to zero. For dataset 1, the data were exported with all delay values set to zero.

PHASE CORRELATION METHOD

Phase correlation relies on the translation property of the Fourier transform, which is referred to as the Fourier shift theorem. Let f_1 and f_2 be two images that differ only by a displacement (x_0, y_0) :

$$f_2(x, y) = f_1(x - x_0, y - y_0) \quad (1)$$

Their corresponding Fourier transforms, F_1 and F_2 , will be related in the following way:

$$F_2(\xi, \eta) = e^{-j2\pi(\xi x_0 + \eta y_0)} \times F_1(\xi, \eta) \quad (2)$$

where ξ and η are spatial frequencies in the x and y directions, respectively.

The cross-power spectrum of two images f_1 and f_2 with Fourier transforms F_1 and F_2 is defined as:

$$\frac{F_1(\xi, \eta) \times F_2^*(\xi, \eta)}{|F_1(\xi, \eta) \times F_2(\xi, \eta)|} = e^{j2\pi(\xi x_0 + \eta y_0)} \quad (3)$$

where F_2^* is the complex conjugate of F_2 . The shift theorem guarantees that the phase of the cross-power spectrum is equivalent to the phase difference between the images. The inverse Fourier transform of the representation in the frequency domain results in an impulse function, i.e., a function that is approximately zero everywhere except at the displacement needed to optimally register the two images (Reddy and Chatterji, 1996). The impulse function can be represented by a two-dimensional matrix P (phase corre-

lation matrix), defined as:

$$P = \begin{bmatrix} c_{0,0} & \cdots & c_{x,0} & \cdots & c_{N-1,0} \\ \vdots & \ddots & \vdots & \ddots & \vdots \\ c_{0,y} & \cdots & c_{x,y} & \cdots & c_{N-1,y} \\ \vdots & \ddots & \vdots & \ddots & \vdots \\ c_{0,N-1} & \cdots & c_{x,N-1} & \cdots & c_{N-1,N-1} \end{bmatrix} \quad (4)$$

where c is the phase correlation coefficient, and the image size is $N \times N$ pixels. If a strongly similar pattern exists in two images but with a translational offset (x_0, y_0) , then c_{x_0,y_0} will have the maximum value within the P matrix and will be a measure of the similarity between the images.

For example, if the true yield map looks like figure 1a, with the operating direction of the harvester indicated by figure 1b, the yield map containing a flow delay error might look like image G (fig. 1c). Images G_1 and G_2 (figs. 1d and 1e) are formed by extracting the appropriate portion of image G , as shown in figure 1c, and then applying translational shifts of 0 and 1 pixels in the x (horizontal in fig. 1) direction to G_1 and G_2 , respectively. Phase correlation of these two images should produce a P matrix with a maximum at $c_{1,0}$, and a relatively smaller value of $c_{0,0}$, indicating that the two images are not particularly similar due to the unaccounted-for flow delay. If we consider another pair of shifted images where the delay time has been correctly accounted for, such as H_1 and H_2 in figures 1f and 1g, then these images will be almost identical. Phase correlation of these two images should also produce a maximum at $c_{1,0}$ but should have a relatively higher value for $c_{0,0}$ than did G_1 and G_2 , indicating that H_1 and H_2 are more similar than G_1 and G_2 .

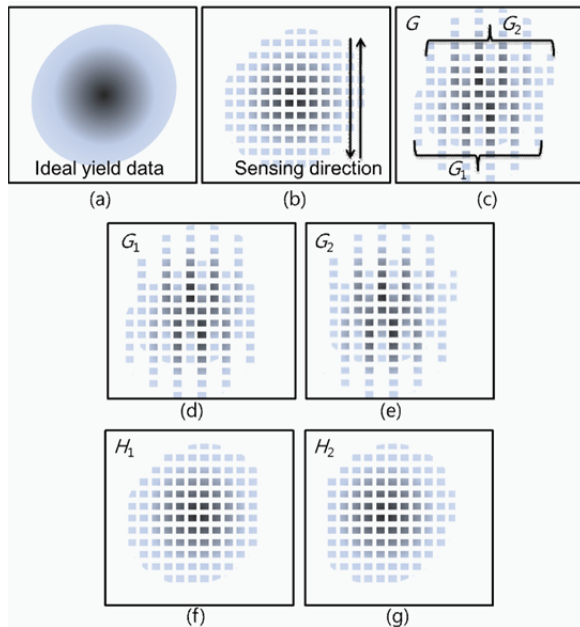


Figure 1. Visualization of paired shifted images taken from an ideal dataset: (a) ideal yield data, (b) discretized data showing sensing direction, (c) illustration of clipping method, (d, e) clipped images with incorrect delay time applied, and (f, g), clipped images with correct delay time applied.

To better evaluate this theoretical case, three ideal images with different assumed delay times (G , H , and I) were generated by digital image processing (figs. 2a, 2b, and 2c). Given the same translational offset as before (1, 0), we can calculate a phase correlation matrix (i.e., P_G , P_H , P_I) for each image. The maximum value in each P matrix should be always found at $c_{1,0}$, as demonstrated by figure 2d. Closer investigation of $c_{0,0}$ (fig. 2e) shows some important variation across the three P matrices. The variation in $c_{0,0}$ then represents the variation in spatial similarity between each pair of images (fig. 2f). Given this fact, it should be possible to determine the true delay time by finding the maximum $c_{0,0}$ calculated across a reasonable range of delay times.

To test the method on non-ideal data, a subset region of dataset 1 was converted to a two-dimensional square raster image by simple mapping of each individual yield observation to its nearest pixel. Pixels were scaled to be of equal size in both dimensions and were based on the larger spatial dimension of the dataset, with extra pixels in the smaller spatial dimension simply padded to zeros. The number of pixels in the raster image was chosen to be somewhat larger than the total number of yield data points. This was done to ensure that very few pixels would contain multiple spatial observations (which were averaged), while minimizing the number of pixels that included no observations (which were set to zero). In this case, where the subset area contained 4,640 sampling points, the appropriate size of the square image was determined to be 128×128 pixels. The translational offset applied was (1,0), as that direction was determined to be perpendicular to the harvest transects. In calculation of the Fourier transform, no windowing or smoothing was applied, to avoid the imposition of additional variability in the yield data. Raster maps for delays ranging from -32 s to +32 s were created in the clipped image, and phase correlation analysis was applied to these maps. Negative delay times were included because several of the test datasets were exported with a 12 s assumed delay. Thus, if the true overall delay were less than 12 s, a negative delay would be expected in this analysis.

Figure 3a shows the inconsistent behavior of $c_{0,0}$ in this analysis. The reason for this inconsistency was determined to be that over 70% of the pixels in the image included no real spatial data and had been assigned a value of zero. The power of these missing points in the frequency domain interfered with retrieving the relative similarity between two images.

APPLYING GAUSSIAN WHITE NOISE

Gaussian white noise (GWN) has the quality of being independent of time series and spatial relationships. As a result, replacing missing data points with GWN should eliminate any potential spatial relationships in the missing data. Therefore, GWN with variance on the order of magnitude of that in the real data was embedded in those pixels that did not contain actual data during the rasterization process. This modification to the algorithm was based on the following considerations. First, phase correlation of two images from different GWN distributions would be approx-

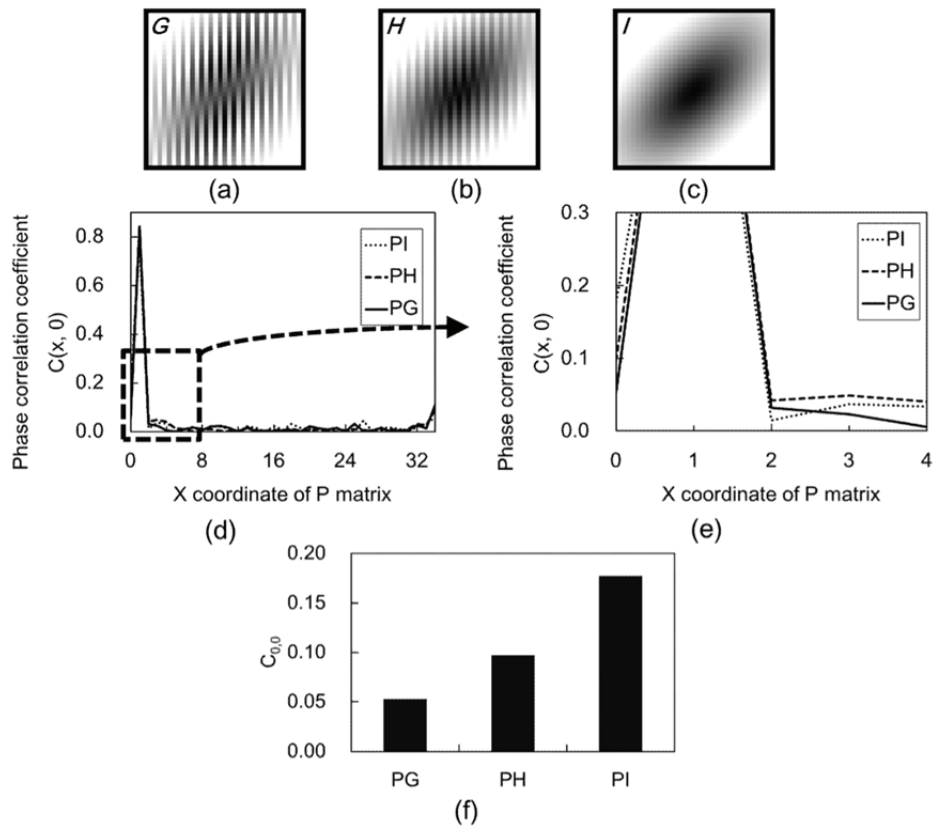


Figure 2. Variation in $c_{0,0}$ across three different delay times for an ideal data set: ideal yield maps with delay times simulated with (a) large error, (b) smaller error, and (c) zero error; overall (d) and magnified (e) plots of the first row of the phase correlation matrix; and (f) plot of $c_{0,0}$ for different delay times, showing a maximum value at the correct delay.

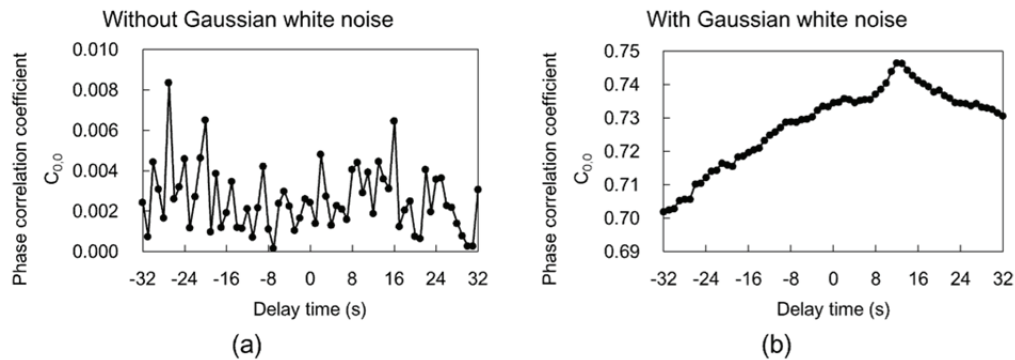


Figure 3. Phase correlation coefficient results for (a) original test dataset and (b) test dataset with embedded Gaussian white noise.

imately 0 in every element of P . Secondly, two images generated from the same GWN distribution (and thus identical) would result in every element of the P matrix having a value of 0 except for $c_{0,0}$, which would always be 1. Embedding the same GWN into the missing pixels of any two images G_1 and G_2 would cause the power of missing points in the frequency domain to be removed and the geographical similarity of the true spatial dataset to be the only factor affecting change of the $c_{0,0}$ value. After removing the effect of the missing pixels, the P matrix will represent only the spatial similarity between G_1^* and G_2^* (where $*$ indicates images imbedded with the same GWN). The largest element in the P matrix will generally be found at $c_{0,0}$. The magnitude of $c_{0,0}$ calculated by this phase correlation method on G_1^* and G_2^* represents the relative spatial homogene-

ity of the data.

Using the same sample data from dataset 1, we created G_1^* and G_2^* by embedding identical GWN patterns into the missing pixels of G_1 and G_2 , differing only by a translation of (1, 0), as shown in figure 4. This procedure moved the maximum peak value in the P matrix back to $c_{0,0}$. The procedure was repeated across the range of delay times, and the resulting range of $c_{0,0}$ values was computed and compiled. The addition of GWN to the missing pixels produced a clear maximum in $c_{0,0}$ for this dataset at approximately 14 s delay time (fig. 3b).

With the addition of GWN, the relationship between $c_{0,0}$ and the spatial similarity of two yield data images (G_1^* and G_2^* , fig. 4) became apparent. Thus, we used the value of $c_{0,0}$ as an index of relative spatial consistency (RSC) at a

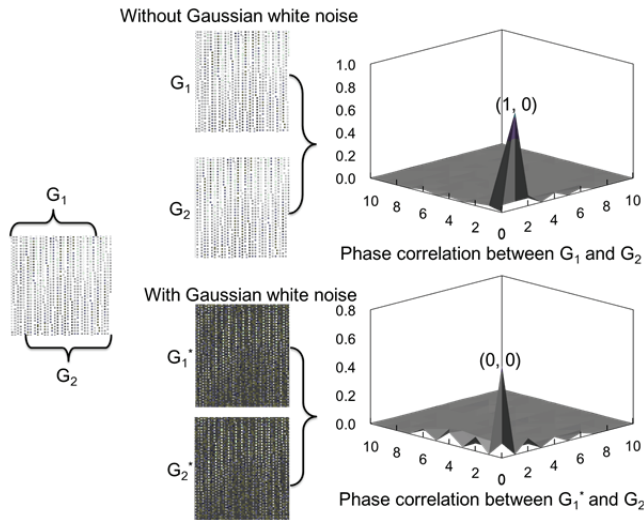


Figure 4. Effect on P matrix of embedding Gaussian white noise.

given delay time. The best delay time is found at the maximum RSC across the range of delay times tested. The value of RSC is relative within a single spatial dataset with a single imbedded GWN distribution, and quantitative comparisons across datasets or different GWN distributions are not valid.

PIXEL COUPLING

To eliminate additional variability in the method, pixels were identified as either valid (containing one or more valid spatial points) or invalid (containing no spatial points). When two translated images G_1^* and G_2^* had a corresponding pixel that was valid for both images, we referred to that as a coupled pixel. When either of the corresponding pixels was invalid, the pixel was replaced in both G_1^* and G_2^* by the same GWN value, thus minimizing its impact during the phase correlation computation. Figure 5 demonstrates the reduction in variability of the RSC across delay times for sample dataset 2 when pixel coupling was ignored (fig. 5a) versus when pixel coupling was a part of the pre-processing procedure for phase correlation (fig 5b). The inclusion of pixel coupling completed the conceptual basis for the development of the phase correlation delay identification (PCDI) method.

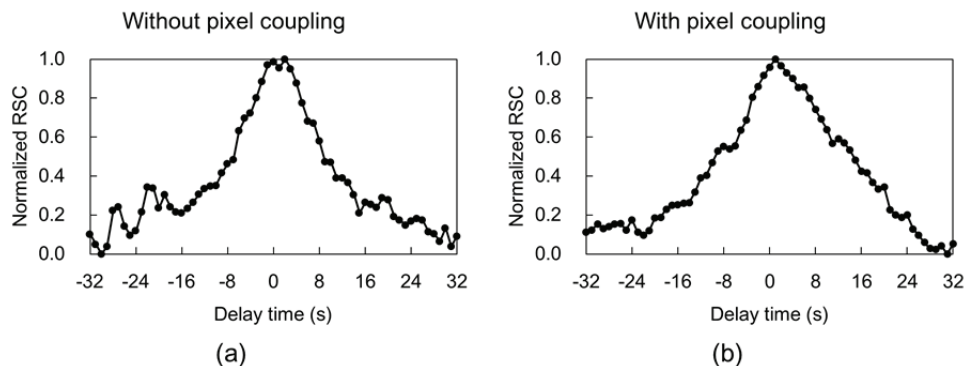


Figure 5. Comparison of relative spatial consistency (RSC) from phase correlation method applied to a test dataset (a) without pixel coupling and (b) with pixel coupling.

DETERMINING RASTERIZATION SIZE

To develop an automated, optimized PCDI method, it was essential to determine the best rasterization size (and thus pixel size) of the image representing the spatial dataset without the need for manual observation of the data. The rasterization process can be thought of as sampling by a unit-impulse (delta) transfer function that transformed the yield monitor data obtained on transects sampled at a constant time interval to a grid of data on a constant spatial (i.e., X - Y) interval. The approaches described below were implemented to minimize information loss due to this discrete sampling process.

The best rasterized image should theoretically include the same number of pixels as actual yield monitor data points, with exactly one pixel for each raster cell, although in practice this is not possible. Generally, if there are too many pixels (i.e., pixel size $< 1/2$ header width), there are not enough coupled pixels in adjacent transects for phase correlation to be effective. On the other hand, with too few pixels (i.e., pixel size $>$ header width), the associated averaging of adjacent transects may leave no spatial structure for the PCDI method to detect. Usually, harvest data will include information about the combine header width or cutting swath width, which could be used to automatically determine the optimal pixel size. However, in order to make the PCDI method more general and suitable for other types of spatial data with inherent time delays but perhaps unrelated to combine operations, a different approach was required.

It would be preferable for the rasterization process to maximize the number of both the valid pixels and the coupled pixels in the image. To concurrently examine the relationships between these, the ratio of valid pixels and the ratio of coupled pixels were calculated for each test dataset across the range of rasterization sizes using the following equations:

$$\text{Ratio of valid pixels} = \frac{\text{Number of valid pixels}}{\text{Number of spatial data points}} \quad (5)$$

$$\text{Ratio of coupled pixels} = \frac{\text{Number of coupled pixels}}{\text{Number of valid pixels}} \quad (6)$$

The intersection point of these two ratios (indicated by the dotted circles in fig. 6) provided a starting point for the

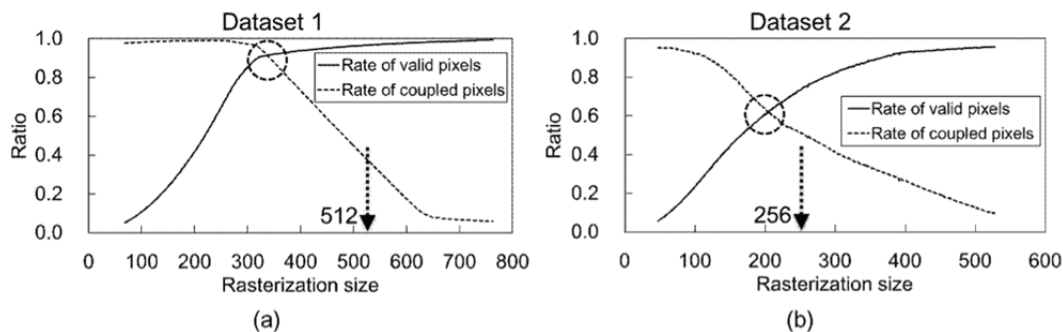


Figure 6. Plots of the ratio of valid pixels and the ratio of coupled pixels for (a) dataset 1 and (b) dataset 2.

selection of rasterization size. To implement the fast Fourier transform performed as a part of phase correlation, a square image whose size was an even power of 2 was required. Based on results from the test datasets, we found that the next larger power of 2 beyond this intersection point provided consistently good outcomes, with the resultant pixel size generally between about 50% and 85% of the combine header width. Values in this range ensured that point data from adjacent passes generally fell into adjacent pixels in the image.

DETERMINING TRANSLATIONAL OFFSET

Once rasterization for a particular dataset was complete, the last thing to be determined was the translational offset to be applied between G_1^* and G_2^* . Since the rasterization procedure was designed to create an image with a significant number of coupled pixels belonging to adjacent transects, the only translations that could shift a large number of pixels directly onto an adjacent transect consisted of the set $\{(1,0), (0,1), (1,1)\}$. While the optimal of these three values could often be identified by visual inspection of harvest direction, in reality most datasets will contain multiple harvest directions for a variety of reasons (e.g., end rows, field roads, terraces, circular planting on a pivot).

The following technique was used to determine the best translational offset and was applied to the sample datasets shown in figure 7. The PCDI method was applied to the three sample datasets shown, with translations of (1,0), (1,1), and (0,1), respectively. The resulting RSC for each of the three translations was computed across the delay range of -32 s to +32 s. These results (fig. 7) showed that a translation of (1, 1) consistently provided good results, even when the dataset clearly contained primarily vertical or horizontal transects. This is because using the translation (1,1), even when the translations (1,0) or (0,1) would be more appropriate, still offsets the adjacent transects properly. While it also moves the pixels slightly along the axis of combine travel, assuming that there is some spatial structure in the data, this should still maximize the correlation between the two images at the proper delay time. Furthermore, in fields that contain data harvested in both a vertical and horizontal direction (e.g., end rows), both types of data are shifted over adjacent transects, which provides the best opportunity to detect the proper delay time.

METHOD EVALUATION

The PCDI method described above was developed using

MATLAB 7.11 (The MathWorks, Inc., Natick, Mass.) using the functions `fft2d` and `ifft2d` to perform the fast Fourier and inverse fast Fourier transformations for phase correlation. Once implemented, the PCDI method was tested on the six initial datasets described in table 1. In contrast to the small subsamples of dataset 1 used in the method development (figs. 3 and 7), these analyses were done with the complete datasets. For each dataset, the rasterization size was determined as described above. The translational offset was set to (1,1). A single GWN pattern was filled into the invalid pixels of a set of images with delays ranging from -32 s to 32 s on a 1 s interval. Phase correlation was calculated to determine RSC for each of those images. The best delay time for each dataset was then chosen from the image pair that contained the largest RSC value, and the associated delay time was reported.

Estimated delay time by the PCDI method was compared with delay time determined by our previously developed geostatistical method (Chung et al., 2002) and delay time obtained using visual methods, as described by Chung et al. (2002) and Sudduth and Drummond (2007). In an approach similar to the RSC, the geostatistical method examined the nugget variance, the variogram parameter that represents the amount of small-scale variation in a spatial dataset. The nugget value was minimized at the true delay time, assuming that most actual yield variations are relatively smooth and well-behaved (Chung et al., 2002). In the visual method, yield maps were subjected to scrutiny by an expert in the processing of yield map data, and delay times were estimated by visual inspection. Further, the expert rated each map on a scale of 1 to 10 with his confidence that his delay estimate was correct. A value of 10 indicated that the expert was virtually certain that his delay estimate was correct. A value of 1 indicated that the estimate was an educated guess.

For further evaluation of the PCDI method, we tested the fully automated method on a much larger set of 50 yield maps. These were sampled from a data warehouse of yield maps stratified by producer ($n = 7$), year (variable per producer), and crop (corn or soybean). This selection ensured a variety of field configurations and harvest patterns; multiple combines, operators, and yield monitors; variability in crop harvesting conditions; and a range in the required delay corrections. The range of delay times investigated was -8 s to 18 s, which encompassed the range of delays likely when using a reasonable initial export delay. This approach also guarded against potential aliasing that could occur on

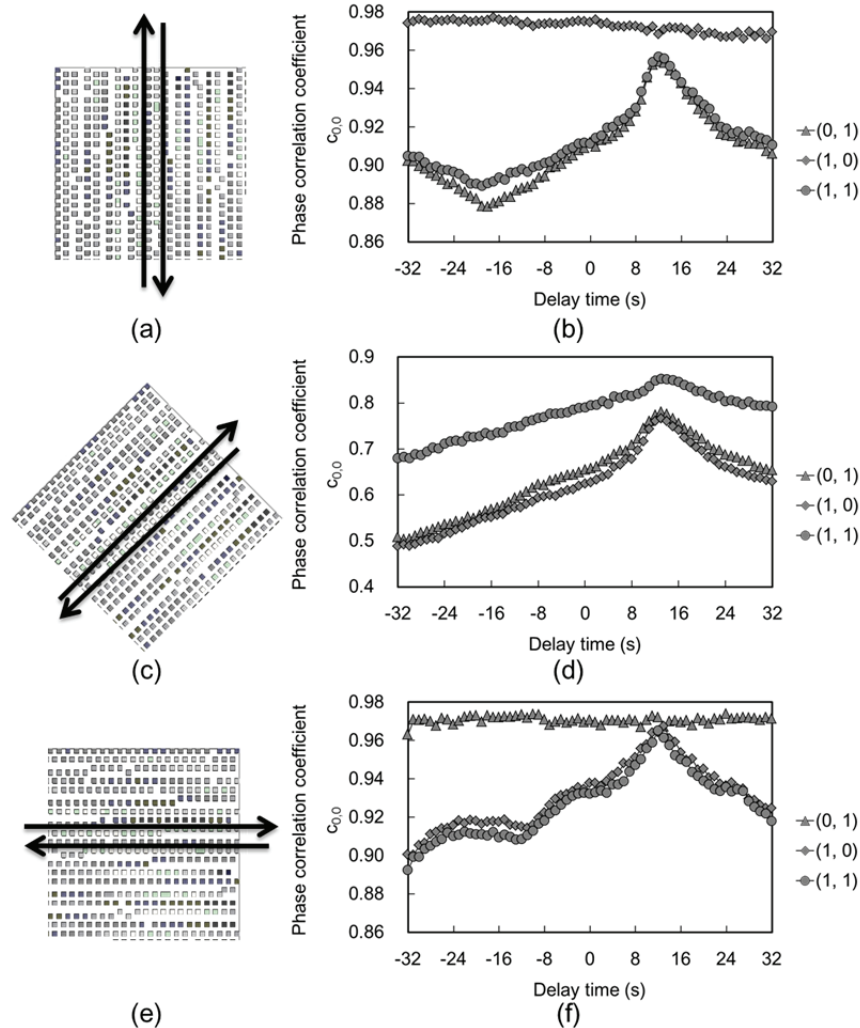


Figure 7. RSC obtained with different translational offsets on test data rotated by (a,b) 0°, (c,d) 45°, and (e,f) 90°.

particularly small fields where transects might be on the order of 20 s or less in length. In preliminary tests with the six initial datasets, we found that the RSC curves obtained with the PCDI method were more variable than the curves obtained with the geostatistical method. As a result, for these tests we ran the PCDI method ten times on each field (with random GWN patterns), both to get a distribution of estimates and to average the RSC curves over the ten iterations. The delay time selected was based on the average RSC curve, although the ten individual estimates were also exported, as was the standard deviation of those ten estimates. The geostatistical method of Chung et al. (2002) was also applied to these data, as were estimates of delay time by the visual inspection method and the associated visual confidence rating.

RESULTS AND DISCUSSION

METHOD EVALUATION WITH SIX INITIAL DATASETS

Values of RSC across the range of delay times for the initial six datasets are shown in figure 8. For comparison, the semivariogram nugget was calculated as a function of delay using the geostatistical method described by Chung et al.

(2002). For this method, the estimated delay time was given by the minimum nugget value.

Particularly for datasets 1 and 4, which have simple harvest patterns and relatively high yield variation, all three methods gave very similar results (table 2). Both automated methods provided curves with well-defined extrema in these datasets (figs. 8a and 8d). Extrema were also quite well-defined for datasets 2, and 6 (figs. 8b and 8f); however, the correspondence between the methods was not as good (table 2). For dataset 2, this can be partially explained by the extremely complex harvest pattern caused by the large number of terraces on the field. Dataset 4 consisted of data from at least two different harvest dates, significantly separated in time and with vastly different grain moisture levels, which may help explain this result. Datasets 3 and 5 (figs. 8c and 8e) were from smaller fields with less yield variability and generally less well-defined time delays. Both fields had a relatively large variation in delay time among the three methods (table 2). For fields with a low level of yield variability, such as these two fields, it was difficult to assess delay time by the visual inspection method. Although the visual method may be considered to provide a more or less “true” delay time in fields with strong patterns of yield variation, this was not the case

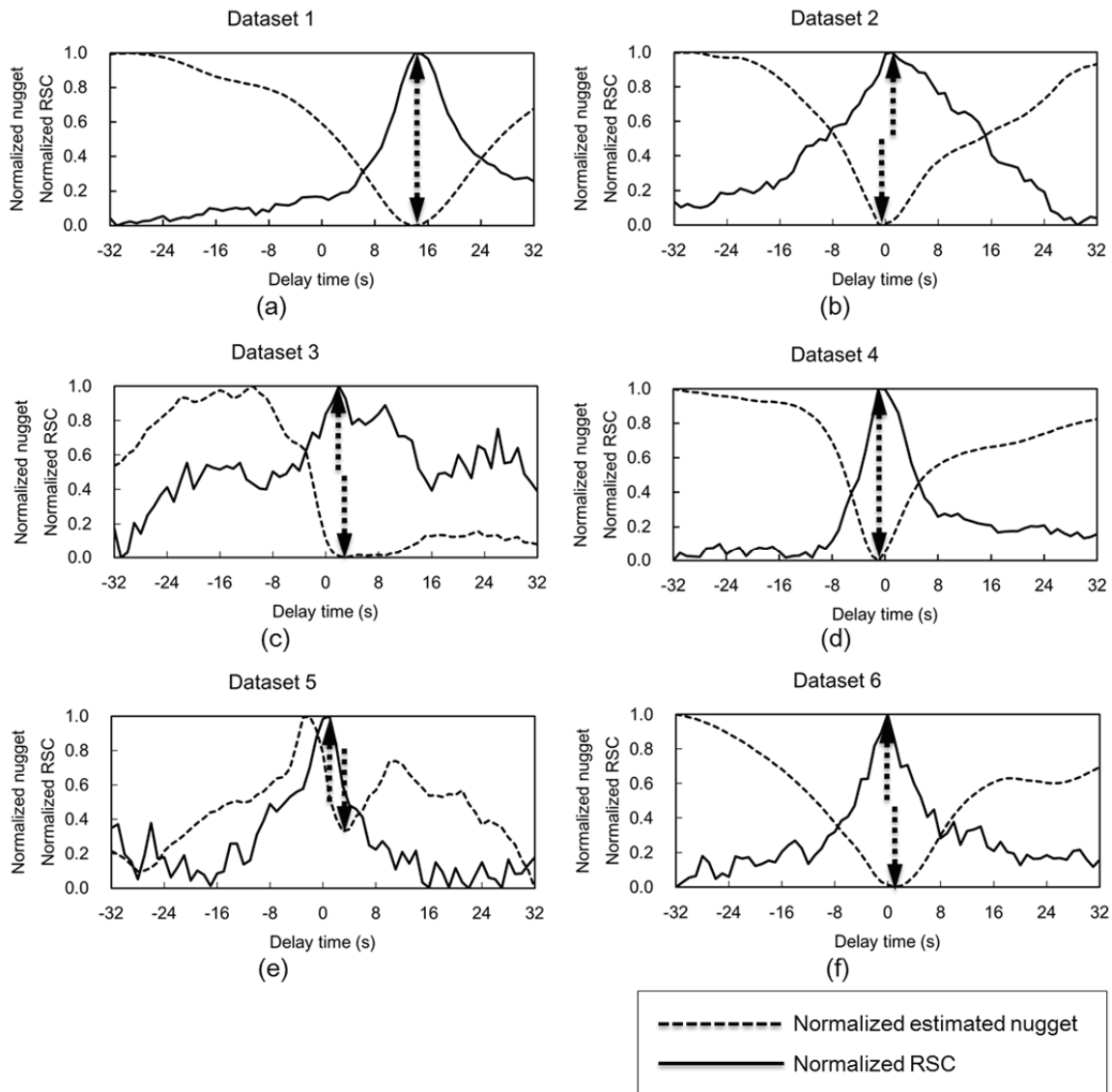


Figure 8. Comparison of normalized estimated nugget and RSC for six initial test datasets across a range of delay times. Correct delay time is indicated by minimum estimated nugget and maximum RSC.

for these fields. Thus, in this case, it is difficult to say that any one of the three methods was correct or incorrect, only that they provided different results.

The PCDI method provided one significant improvement over the other methods. In each instance, it could compute the delay time in well under 7 s on a standard desktop com-

puter with Microsoft Windows XP and an Intel Core2 processor at 2.83 GHz. The geostatistical method proposed by Chung et al. (2002) took longer to execute on the same computer, requiring nearly 22.5 min to compute the result on the largest dataset (dataset 4). This difference can be explained by a comparison of the computational complexity of the two methods. The geostatistical method requires one or more computations for each separate pair of the M points in a dataset, for a computational complexity of at least order M^2 . A 2D FFT, which is the most complex part of the PCDI method, has a complexity of order $N^2 \times \log(N^2)$, where $N \times N$ is the size of the raster image (Brenner and Rader, 1976). In the best case, for a perfectly square field of evenly spaced observations, $N = M^{1/2}$. In this case, the PCDI method complexity would reduce to order $M \times \log(M)$, a significant improvement over the geostatistical method.

Table 2. Delay time by phase correlation delay identification (PCDI), geostatistical, and visual methods for initial test datasets.

Dataset	Delay Time Determined by Each Method (s) ^[a]			Visual Confidence Rating ^[b]
	PCDI	Geostatistical	Visual	
1	14	14	14	7
2	1	-1	1	4
3	2	3	0	1
4	-1	-1	0	6
5	1	4	1	2
6	0	1	-2	4

^[a] Dataset 1 was exported from AgLeader SMS Basic software with no delay. Datasets 2 through 6 were exported with a 12 s delay. Delay time determined here is with respect to that export delay.

^[b] Rating of certainty of correct delay time by the visual method, with 10 being most certain and 1 being most uncertain.

EVALUATION WITH ADDITIONAL DATA

Table 3 presents results from applying the PCDI, geostatistical, and visual methods to the 50 additional datasets.

Table 3. Evaluation results by phase correlation delay identification (PCDI), geostatistical (GS), and visual (VI) methods for 50 additional datasets. Bold entries represent questionable results, defined by column for PCDI and GS columns: difference from VI >3 s; for VI and VC columns: VC < 3; and for PCDI SD column: PCDI standard deviation >3 s).

Combine	Crop	Number of Data Points	Delay Time Determined by Each Method (s) ^[a]				Execution Time (s)		PCDI SD ^[c]
			PCDI	GS	VI	VC ^[b]	PCDI	GS	
621	soybean	15,258	-2	-1	-1	10	5.6	57.8	0.3
038	soybean	8,304	-1	13	-1	10	5.3	18.9	0.3
641	corn	17,804	-1	-1	-1	10	15.5	67.1	0.0
678	corn	13,245	-3	-1	-3	10	5.5	50.1	0.0
621	corn	9,264	-1	-1	-1	9	5.3	29.7	0.0
038	soybean	7,693	-1	-2	-1	9	5.2	12.2	0.4
641	corn	41,432	2	-1	-1	9	17.8	345.7	2.6
465	corn	10,563	4	4	4	9	5.7	25.1	0.0
465	corn	12,621	4	5	4	9	5.5	65.1	0.5
621	corn	15,332	-1	0	-1	8	5.6	52.2	0.0
038	corn	6,970	-1	-1	-1	8	5.1	12.6	0.3
678	corn	15,034	-2	-2	-2	8	5.7	55.3	0.3
641	soybean	14,500	-1	-2	-1	7	5.7	51.8	0.0
621	soybean	12,018	-1	0	-1	6	5.6	45.1	0.0
038	corn	8,057	-1	-1	-1	6	5.3	16.0	0.0
038	corn	10,066	-1	-1	-1	6	5.4	30.2	0.3
621	soybean	13,703	-1	0	-1	5	5.5	49.8	0.4
344	soybean	21,839	1	0	0	5	15.8	91.2	0.5
344	soybean	10,391	-2	-3	-2	5	5.3	30.7	1.1
465	soybean	9,119	4	4	5	5	5.2	28.2	1.1
038	soybean	5,044	-1	-1	-1	4	5.2	7.3	0.0
803	corn	21,847	1	1	1	4	15.7	128.3	0.5
678	corn	11,734	-3	-2	-2	4	5.8	48.4	0.6
621	corn	5,144	0	0	0	3	5.1	8.5	0.0
038	soybean	4,554	-1	-1	0	3	5.0	7.0	0.0
344	soybean	18,293	3	-1	0	3	15.5	82.3	2.3
344	soybean	19,180	2	0	1	3	16.4	85.3	1.1
744	corn	3,544	0	-1	0	3	2.6	3.1	4.1
803	soybean	9,841	1	0	0	3	5.3	22.6	0.5
678	corn	15,683	-2	-2	-3	3	5.6	75.1	0.4
621	corn	10,570	0	18	-2	2	5.3	26.2	0.5
621	soybean	4,669	1	0	0	2	5.0	6.6	0.9
038	corn	551	-1	18	-1	2	1.8	0.2	0.5
344	soybean	32,926	-1	-1	-2	2	16.5	186.5	0.5
744	corn	12,312	-1	0	-1	2	5.5	40.3	0.3
744	soybean	3,576	4	18	-2	2	2.6	3.8	3.7
744	soybean	2,761	-1	-6	-1	2	2.8	1.9	2.2
803	soybean	4,015	12	1	1	2	2.6	3.8	9.5
465	soybean	6,531	3	1	2	2	5.1	13.8	2.5
678	soybean	4,293	-1	-2	-3	2	5.0	5.8	5.9
038	corn	584	0	-1	-1	1	1.8	0.2	4.8
038	soybean	1,777	17	-1	-2	1	2.5	1.2	7.3
344	soybean	1,076	-1	-1	-1	1	2.5	0.5	1.6
344	soybean	1,620	-1	-4	-1	1	2.5	1.0	0.9
744	corn	1,952	-1	18	-1	1	2.5	1.1	0.5
678	corn	9,401	0	16	0	1	5.3	21.1	0.9
678	soybean	13,326	-2	-2	-1	1	5.4	72.5	2.4
678	soybean	2,893	5	-1	-1	1	2.6	3.8	4.6
678	soybean	1,357	11	-2	0	1	2.5	1.3	3.2
678	soybean	3,892	-3	-1	-3	1	2.7	7.1	2.4

^[a] Delay time is relative to the delay used by the producer or crop advisor to export data from the yield monitor; PCDI = phase correlation delay identification, GS = geostatistical method, and VI = visual method.

^[b] Visual confidence rating, with 10 being most certain and 1 being most uncertain.

^[c] Standard deviation of ten estimates obtained using the phase correlation method.

These results were quite promising, with the PCDI method able to select a value within 3 s of the visual method in all but five of the 50 fields. In those five cases, the visual confidence of the expert was rated as either a 1 or 2, indicating very poor confidence in the visual estimate. The geostatistical method was able to produce reasonable estimates in four out of five of these cases, but in an additional six cases estimates by the geostatistical method were clearly not correct, although once again, all but one contained a visual confidence value of either 1 or 2.

As expected, the PCDI method was very quick to compute, with an average time of 6 s to complete the ten passes of the data through the algorithm. The maximum time on the largest fields was 18 s, indicating that the method would likely scale up well to larger datasets. The geostatistical method had an average time of 40 s, and although this average time might be manageable, the maximum time for the largest of these fields was almost 360 s, indicating that the method might not be suitable for larger datasets.

Another advantage of the PCDI method was that run-

ning the algorithm ten times provided a distribution of estimates to consider. Often, the PCDI method gave the same result each time, leading to a standard deviation of zero for the ten estimates. Other times, there were one or two outliers, giving us confidence that the other eight or nine estimates were reasonable, and tending to provide a fairly small standard deviation. For the five times that the PCDI method clearly gave questionable results, the standard deviation of these ten estimates was quite large (>3). In fact, there were only eight fields for which the standard deviation was this large, indicating that it may be possible to know something about the reliability of the overall estimate from the distribution of the individual PCDI estimates.

The PCDI method was packaged as a software component and has been included for automated delay time detection in the beta version of Yield Editor 2.0, our software that detects and removes many error types affecting yield map accuracy. An executable file of Yield Editor 2.0 is available free for download from the USDA-ARS website (www.ars.usda.gov/Services/Services.htm?modecode=36-22-15-00).

SUMMARY AND CONCLUSIONS

We have developed a method for correction of instrument offset or delay in yield maps or similar transect-collected sensor data. The PCDI method is a computationally efficient, easily automated procedure that can accurately determine delay time for individual fields. The PCDI method was developed and evaluated using a large number of yield maps with varying degrees of harvest complexity, two different grain crops, and multiple combines, yield monitors, and operators. Results were compared to previously reported geostatistical and visual inspection methods.

The PCDI method identified delay times consistent with the previously reported geostatistical and visual inspection methods. A major advantage of the PCDI approach is its computational efficiency. Execution times were faster than the visual inspection method and approximately an order of magnitude faster than the geostatistical method on the test fields, and considerably more than that as the dataset size increased. The PCDI method also provides estimates of the confidence in delay identification due to rapid re-analysis capability with multiple random GWN fields. The PCDI method represents a significant advancement over current methodologies to identify and correct measurement delay errors.

REFERENCES

Arslan, S., and T. S. Colvin. 2002. Grain yield mapping: Yield sensing, yield reconstruction, and errors. *Precision Agric.* 3(2):

- 135-154.
- Beal, J. P., and L. F. Tian. 2001. Time shift evaluation to improve yield map quality. *Applied Eng. in Agric.* 17(3): 385-390.
- Birrell, S. J., K. A. Sudduth, and S. C. Borgelt. 1996. Comparison of sensors and techniques for crop yield mapping. *Comp. Elect. Agric.* 14(2-3): 215-233.
- Blackmore, B. S., and C. J. Marshall. 1996. Yield mapping: Errors and algorithms. In *Proc. 3rd Intl. Conf. Precision Agriculture*, 403-416. P. C. Robert, R. H. Rust, and W. E. Larson, eds. Madison, Wisc.: ASA, CSSA, and SSSA.
- Brenner, N., and C. Rader. 1976. A new principle for fast Fourier transformation. *IEEE Trans. Acoustics, Speech and Signal Processing* 24(3): 264-266.
- Broughton, S. A., and K. M. Bryan. 2008. *Discrete Fourier Analysis and Wavelets: Applications to Signal and Image Processing*. Hoboken, N.J.: Wiley.
- Chung, S. O., K. A. Sudduth, and S. T. Drummond. 2002. Determining yield monitoring system delay time with geostatistical and data segmentation approaches. *Trans. ASAE* 45(4): 915-926.
- De Castro, E., and C. Morandi. 1987. Registration of translated and rotated images using finite Fourier transforms. *IEEE Trans. Pattern Anal. Machine Intel.* 9(5): 700-703.
- Lamb, J. A., R. H. Dowdy, J. L. Anderson, and G. W. Rehm. 1997. Spatial and temporal stability of corn grain yields. *J. Prod. Agric.* 10(3): 410-414.
- Massey, R. E., D. B. Myers, N. R. Kitchen, and K. A. Sudduth. 2008. Profitability maps as an input for site-specific management decision making. *Agron. J.* 100(1): 52-59.
- Moore, M. 1998. An investigation into the accuracy of yield maps and their subsequent use in crop management. PhD diss. Silsoe, U.K.: Cranfield University, Silsoe College.
- Reddy, B. S., and B. N. Chatterji. 1996. An FFT-based technique for translation, rotation, and scale-invariant image registration. *IEEE Trans. Image Proc.* 5(8): 1266-1271.
- Reyniers, M., and J. De Baerdemaeker. 2005. Comparison of two filtering methods to improve yield data accuracy. *Trans. ASAE* 48(3): 909-916.
- Robinson, T. P., and G. Metternicht. 2005. Comparing the performance of techniques to improve the quality of yield maps. *Agric. Sys.* 85(1): 19-41.
- Stott, B. L., S. C. Borgelt, and K. A. Sudduth. 1993. Yield determination using an instrumented Claas combine. ASAE Paper No. 931507. St. Joseph, Mich.: ASAE.
- Sudduth, K. A., and S. T. Drummond. 2007. Yield editor: Software for removing errors from crop yield maps. *Agron. J.* 99(6): 1471-1482.
- Veal, M. W., S. A. Shearer, and J. P. Fulton. 2010. Development and performance assessment of a grain combine feeder house-based mass flow sensing device. *Trans. ASABE* 53(2): 339-348.
- Whelan, B. M., and A. B. McBratney. 2002. A parametric transfer function for grain flow within a conventional combine harvester. *Precision Agric.* 3(2): 123-134.
- Yang, C., J. H. Everitt, and J. M. Bradford. 2002. Optimum time lag determination for yield monitoring with remotely sensed imagery. *Trans. ASAE* 45(6): 1737-1745.